Mechanics of Materials 161 (2021) 104016

Contents lists available at ScienceDirect

Mechanics of Materials

journal homepage: www.elsevier.com/locate/mechmat

Viscoelasticity and the Small Punch Creep Recovery Test: Numerical analysis and experimental tests on the applicability for polyvinyl chloride (PVC)☆

Jose Calaf-Chica *, Pedro Miguel Bravo Díez **, Mónica Preciado Calzada ***

Research Group of Material Science and Engineering (CIMa), University of Burgos, Avenida Cantabria s/n, E09006, Burgos, Spain

ARTICLE INFO

Keywords:
Small punch test
SPT
Viscoelasticity
Polymer
PVC

ABSTRACT

Research on the Small Punch Test (SPT) has been mainly focused on metallic alloys, with limited investigations in polymeric materials. The miniature size of the SPT eases and motivates its use in biomedical applications, like the mechanical characterization of surgical implants made of different polymers. It is noted that the aim of these publications was focused on mechanical properties inherent to the tensile test (yield strength, ultimate tensile strength, Young's modulus, etc.), but the applicability of this miniature test for the estimation of singular polymer properties like viscoelasticity or viscoplasticity has not been addressed.

The aim of this paper was the assessment of SPT as a characterization test for the viscoelastic properties of polymers. To analyze this applicability, numerical FEM simulations of hypothetical materials were performed and a novel Small Punch Creep Recovery Test (SPCRT) was designed. These FEM simulations were verified with experimental compressive creep recovery tests and SPCRTs for specimens made of polyvinyl chloride (PVC). The results showed that SPCRTs accurately estimated the viscoelastic properties for materials with non-stress-dependent viscoelastic properties. In the case of materials with stress-dependent viscoelastic properties, the SPCRT would estimate a mean or intermediate value of these stress-dependent viscoelastic properties.

1. Introduction

Monitoring of the aging or degradation of the mechanical properties on in-situ structures is difficult by standard testing. The required volume to manufacture the specimens for tensile or fracture testing exceeds the component itself or limits the testing trials. Miniature testing includes a set of alternative methods to estimate the mechanical properties of materials with a minimum affected volume (Karthik et al., 2016), being an alternative testing method in the evaluation of in-situ components or structures. Their applicability has been analyzed and demonstrated in different sectors like the nuclear industry (Manahan et al., 1981; Bruchhausen et al., 2016) or biomedical engineering (Giddings et al., 2001). Special mention must be made of the specific case of the small punch test (SPT). This miniature test has shown exponential development in the last decade. It shows applicability for the estimation of a wide selection of mechanical properties: Young's modulus (Chica et al., 2017), yield strength (Calaf-Chica et al., 2020; Yang et al., 2015), ultimate tensile strength (Altstadt et al., 2018; Simonovski et al., 2018), fracture toughness (Li et al., 2019; Hurst et al., 2019), creep (Cao et al., 2021; Wang et al., 2020a), ductile-to-brittle transition temperature (Altstadt et al., 2021; Wang et al., 2020b), fatigue (Lewis et al., 2019; Lancaster et al., 2019), etc. The use of the SPT has been intensely analyzed for different metallic materials: steels (Chen et al., 2020; Yao and Dai, 2021), titanium (Lancaster et al., 2015; Xue et al., 2019),

Abbreviations: E, Elastic modulus; γ, Correlation coefficient; $Slope_{ini}$, Maximum slope at the initial stages of the SPT curve; $Slope_{UL}$, Slope of the unloading curve of the SPT curve; σ_y, Yield strength; σ_u, Ultimate tensile strength; θ_1 and θ, β_1 and β_{22}, Correlation coefficients; P_y, Yield load; t_s, Specimen thickness; P_m, Maximum load of the SPT curve; δ_m, Punch displacement at maximum load of the SPT curve; P_i, Intersections load of the SPT curve; G, Shear modulus; K, Bulk modulus; α, Relative modulus; τ, Relaxation time; t, Time; υ, Poisson's ratio; $k(t)$, Time-dependent stiffness of the recovery phase; δ, Punch displacement.

☆ Note: This research did not receive any specific grant from funding agencies in the public, commercial, or not-for-profit sectors.

* Corresponding author.
** Corresponding author.
*** Corresponding author.
E-mail addresses: jcalaf@ubu.es (J. Calaf-Chica), pmbravo@ubu.es (P.M. Bravo Díez), mpreciado@ubu.es (M. Preciado Calzada).

https://doi.org/10.1016/j.mechmat.2021.104016
Received 25 April 2021; Received in revised form 5 July 2021; Accepted 5 August 2021
Available online 12 August 2021

aluminum (Gao et al., 2020; CALAFCHICA et al., 2021), copper (Ghodke et al., 2020), nickel (Taheri et al., 2021) alloys, etc. Its applicability for polymers and ceramic materials has been also investigated but showing less research continuity (Rasche et al., 2014; Shindo et al., 2003; Rodríguez et al., 2016), with promising publications in the 90s and most recent research in the last years.

The SPT is an axisymmetric test (see Fig. 1(a)) which consists of a circular plate specimen with a thickness of 0.5 mm and a minimum diameter of 8.0 mm. This disc is clamped between two dies and punched until failure by a ball with a diameter of 2.5 mm ((2013). F2977-13: S, 2013a). The key to this miniature test is its reduced size and simplicity, allowing the testing of small components (like orthopedic bearings), or huge structures by a quasi-non-destructive methodology. Fig. 1(b) shows the registered data during the test: the punch load versus the punch displacement, commonly named as the SPT curve. The displacement data may be registered using an extensometer fixed to the upper and lower arms of the testing machine (known as punch displacement) or maybe registered using an LVDT transducer in contact with the lower face of the SPT specimen (named as specimen deflection).

The different mechanical properties are estimated from the SPT curve with different methodologies, which generally use correlation equations that relate the mechanical property (e.g., yield strength) with data extracted from the SPT curve (e.g., the yield load) (Yang et al., 2015). In most cases, these equations show linear relationships and the coefficients of these correlations must be empirically deduced with previous standard tests and SPTs for similar materials. The coefficients of these correlation equations are obtained empirically with a comparison between standard tests and SPTs with specimens extracted from the same raw materials. This correlation equation is used to estimate the mechanical properties of materials within the limits ranged in the previous empirical estimation.

The mechanical properties inherent in the standard tensile test are estimated in the SPT by different methodologies:

(a) Young's modulus estimation:

I. Initial slope of the SPT curve (see Fig. 2(a)). This method uses the maximum slope ($Slope_{ini}$) reached at the first stages of the SPT curve. A linear correlation is established between these maximum slopes and the Young's modulus for a set of materials in order to obtain the empirical coefficients (γ) of the linear correlation (see equation (1).

$$E = \gamma \cdot Slope_{ini} \tag{1}$$

II. Unloading/loading slope of the SPT curve (see Fig. 2(a)). An unloading/loading stage is included in the testing procedure for a punch displacement of 0.1 mm. The slope of the unloading curve ($Slope_{UL}$) is linearly correlated with the Young's modulus with the equation (2). This method reduces the dependency of γ coefficient with the plastic properties of the material in comparison with the method I.

$$E = \gamma \cdot Slope_{UL} \tag{2}$$

(b) Yield strength estimation:

I. Mao's method (see Fig. 2(a)). This method draws two tangents at: the maximum slope of initial stages of the SPT curve, and the minimum slope reached at mid-stage of the SPT curve. The load of the crossing point of these two tangents is named as the yield load (P_y) and it is correlated linearly with the yield strength of the material with the equation (3).

$$\sigma_y = \theta_1 \cdot \frac{P_y}{t_s^2} + \theta_2 \tag{3}$$

II. t/10 offset method (see Fig. 2(a)). This method draws an offset line parallel to the maximum slope of initial stages of the SPT curve (offset equal to the tenth of the specimen thickness). The load of the crossing point between this offset line and the SPT curve is named as the yield load (P_y), and it is linearly correlated with the yield strength with the same empirical equation (3) used for the Mao's method.

(c) Ultimate tensile strength estimation:

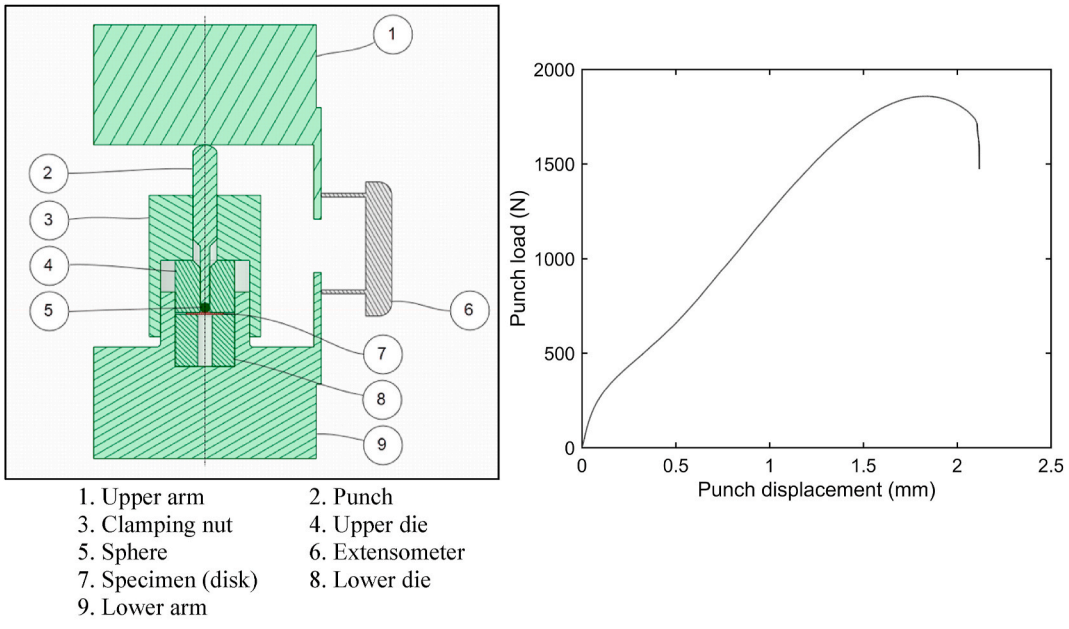

Fig. 1. (a) SPT set-up and (b) experimental SPT curve.

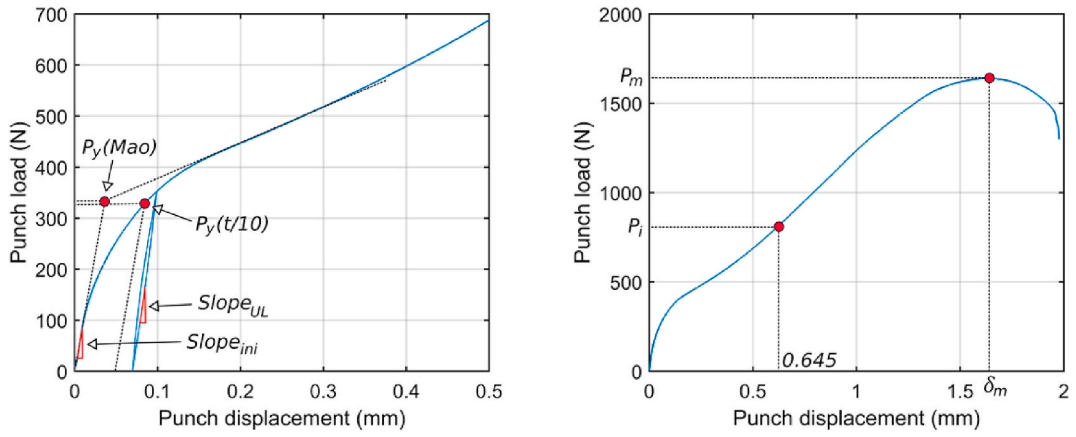

Fig. 2. Estimation methods for: (a) Young's modulus and yield strength and, (b) ultimate tensile strength.

I. Maximum load method balanced with the displacement (see Fig. 2 (b)). The maximum load P_m reached during the SPT and the displacement δ_m reached at this maximum load are used to estimate the ultimate tensile strength of the material with the correlation equation (4).

$$\sigma_u = \beta_1 \cdot \frac{P_m}{t_s \cdot \delta_m} + \beta_2 \tag{4}$$

II. Intersections method (see Fig. 2(b)). This method uses the load reached at a fixed displacement of 0.645 mm (intersection load P_i) with the correlation equation (5).

$$\sigma_u = \beta_1 \cdot \frac{P_i}{t_s^2} \tag{5}$$

The first investigation related to the applicability of the SPT to estimate the mechanical properties of polymers was published by Kurtz et al., in 1997 (Kurtz et al., 1997). The authors linked the initial slope of the SPT curve with Young's modulus of ultra-high-molecular-weight polyethylene (UHMWPE). They used the finite element method (FEM) to simulate the SPT behavior for hypothetical materials with different Young's moduli, finding a linear relationship between Young's modulus and the initial slope of the SPT curve. Experimental tensile tests and SPTs of UHMWPE were performed to verify the conclusions obtained with the previous numerical analysis. From this investigation, it is interesting to highlight that by applying a cyclic loading in the SPT, a significant creep behavior was observed. For this cyclic test, an initial punch displacement of 0.06 mm was applied, and unloading-loading cycles with a fixed upper load were established to detect this creep behavior. In 2001, Edidin and Kurtz (2001) published an investigation related to the application of the SPT for evaluating UHMWPE total joint replacement components. In this research, the total energy required to fracture the SPT specimens was related to wearing mechanisms in total hip replacements. The SPT was used extensively for this medical application in later investigations until the publication of the standard ASTM F2183 "Standard Test Method for Small Punch Testing of Ultra-High Molecular Weight Polyethylene Used in Surgical Implants" ((2008). F2183 - 02:, 2008) and the standard ASTM 2977 "Standard Test Method for Small Punch Testing of Polymeric Biomaterials Used in Surgical Implants" ((2013). F2977-13: S, 2013b). Giddings et al. analyzed the applicability of the SPT as a test technique for characterizing Young's modulus of polymethylmethacrylate (PMMA) in total joint replacements to anchor implants (Giddings et al., 2001). Jaekel et al. performed similar investigations for the applicability of the SPT in the characterization of polyetheretherketone (PEEK) polymeric biomaterials (Jaekel et al., 2011), and Kurtz et al. deepened within the use of the SPT to characterize polycarbonate urethane (PCU) (Kurtz et al., 2010). All this research was focused on polymers with biomedical applications, but the analysis of the SPT applicability for polymer materials in a generic sense has been performed in the last years: PLA-nanocomposite films (Rodríguez et al., 2014; Maspoch et al., 2015), polypropylene (PP), polyethylene terephthalate (PET), poly (lactic acid) and ethylene vinyl alcohol (EVOH) (Rodríguez et al., 2016). The most recent research on this issue was published in 2019 by Koga et al. (2020) with an investigation related to the characterization of polyvinyl chloride (PVC) with the SPT.

The SPT was developed in the nuclear industry in the '80s, focused on ferrous metallic alloys. This initial research was extended to other metallic alloys, based on aluminum, copper, or nickel. This is why the most characterized properties with the SPT were the inherent mechanical properties estimated by tensile tests (Young's modulus, yield strength, ultimate tensile strength, and elongation at fracture), fracture tests (fracture toughness), fatigue tests (S–N curves), impact tests (ductile-to-brittle transition temperature) or high temperature creep tests (strain-time curves). At the coming of the SPT in the characterization of polymers, other material properties could be analyzed: estimation of the viscoelasticity and viscoplasticity. This paper aimed to analyze whether SPT could be applicable for the estimation of the viscoelastic properties of polymeric materials.

2. Materials and methods

To assess the applicability of the SPT for the estimation of the viscoelastic properties of polymers, a preliminary study based on the finite element method (FEM) was performed to facilitate the set-up of a later experimental test. For this purpose, the time-dependent stress-strain state of viscoelastic materials was approached using the Prony series. G shear and K bulk moduli were represented with functions of time (see equations (6) and (7)).

$$G(t) = G_0 \left[1 - \sum_{i=1}^{N} \alpha_i^G \left(1 - e^{-\frac{t}{\tau_i^G}} \right) \right] \tag{6}$$

$$K(t) = K_0 \left[1 - \sum_{i=1}^{M} \alpha_i^K \left(1 - e^{-\frac{t}{\tau_i^K}} \right) \right] \tag{7}$$

where.

τ_i^G τ_i^K are the relaxation times for each Prony component G_i or K_i.

α_i^G α_i^K are the relative moduli for each Prony component, where $\alpha_i^G = G_i/G_0$ and $\alpha_i^K = K_i/K_0$

The SPT generates a heterogeneous stress-strain field along with the specimen, with yielded zones at the indentation area just under the spherical puncher while there are zones with lower stresses (below the yield strength) at the outer diameter of the specimen. Yielding is introduced in the material just at the first time of the test. Thus, it is not possible to perform an SPT without yielding the specimen. This is why elastic-plastic properties had to be included in the FEM simulation. For this purpose, an elastic-perfectly-plastic model was used with the mechanical properties selected in Table 1. As a simplification, a single Prony component was selected in the viscoelastic model ($N = M = 1$; see equations (6) and (7)), with similar relative moduli for shear and bulk relaxations. Four α and two τ were selected to generate eight different hypothetical materials.

The SPT estimates the mechanical properties with correlations that relate each mechanical property with different data or parameters extracted from the SPT curve. For the specific case of the viscoelastic model based on Prony series, relative moduli and relaxation times quantify how the elastic properties change over time. Calaf-Chica et al. (2017) demonstrated that unloading slopes in the SPT curve (a measurement of the elastic SPT stiffness) could be linearly correlated with Young's modulus of the material. Thus, punch displacement versus time curve in an SPT could be used as a creep or relaxation test considering the linear correlation between the time-dependent elastic modulus (relaxation modulus in a standard relaxation test) and the time-dependent elastic stiffness in an SPT. Fig. 2 shows the strain-time curve of a standard creep recovery test. In this type of test, a constant load is applied in a tensile or compressive specimen for a specific time. Initially, there is an instantaneous elastic strain ε_0 generated by the application of the constant load. During the first creep phase, viscoelastic and viscoplastic properties increase the strain of the specimen. When the constant load is removed, the elastic strain ε_0 is "instantaneously" recovered and the induced viscoelastic strain ε_{ve} during creep phase is also recovered over time. The remaining strain after this recovery phase corresponds to the viscoplastic strain ε_{vp} generated during the creep phase.

The recovery phase that is initiated at point B (see Fig. 3) could be used to quantify the viscoelastic properties of the material because there are not any viscoplastic alterations after this point. Thus, the initial elastic modulus at point C would be:

$$E_C = \frac{\sigma_B}{\varepsilon_B - \varepsilon_C} = \frac{\sigma_B}{\varepsilon_0} \tag{8}$$

Just after the point C, the strain used to calculate the time-dependent elastic modulus would be incremented by the viscoelastic contribution:

$$E(t) = \frac{\sigma_B}{\varepsilon_B - \varepsilon(t)} \quad t \geq t_C \tag{9}$$

Fig. 4 shows the representation of the time-dependent elastic modulus obtained from data included in Fig. 3 and using the equation (4).

The Prony components (α_i and τ_i) could be estimated with a non-linear least squares regression, based on equation (10) (similar to equation (6)), and the experimental data obtained in Fig. 4.

$$E(t) = E_C \left[1 - \sum_{i=1}^{N} \alpha_i^G \left(1 - e^{-\frac{t - t_C}{\tau_i^E}} \right) \right] \tag{10}$$

Similarly, designing and performing a Small Punch Creep Recovery Test (SPCRT) following the same phases performed in a standard creep recovery test, the recovery phase of this hypothetical SPCRT could be used to perform a non-linear least squares regression based on an equation similar to the equation (6), to estimate the equivalent Prony components of a viscoelastic material. This idea would be supported in the existence of a linear correlation between the elastic modulus and the SPT unloading curve stiffness demonstrated in (Chica et al., 2017).

To demonstrate the applicability of an SPCRT, a FEM simulation of this novel test was performed in ANSYS software. Fig. 5 shows the meshing used for the SPT simulation. A quarter of the 3D model was used taking the advantage of symmetries of the test. Frictional contacts were established between all parts with a frictional coefficient of $\mu = 0.1$.

The simulation was divided in four steps, to emulate a creep recovery test with the SPT:

(a) Step 1. The spherical punch is displaced 0.10 mm in 0.1 s. This step yielded the specimen without enough time to initiate any significant viscoelastic strain. The end of this step would correspond with point A of Fig. 3.
(b) Step 2. The maximum load reached in the previous step 1 was kept constant for 60 s. The end of this step would correspond with point B of Fig. 3.
(c) Step 3. The load of step 2 was reduced to 0.01 N in 0.1 s. The end of this step would correspond with point C of Fig. 3.
(d) Step 4. The minimum load of 0.01 N was kept constant for 60 s. The punch displacement-time curve obtained during this final step would be used to estimate the Prony components (α_i and τ_i) established in the material properties of each hypothetical specimen (data included in Table 1).

To validate the novel SPCRT testing method developed numerically, experimental tests (compressive testing and SPCRTs) were done with specimens extracted from a rod bar (diameter of 10.2 mm) of polyvinyl chloride (PVC). All tests were performed in a Zwick/Roell KAPPA 050 DS testing machine with a load cell Xforce P with a nominal force of 5 kN. For compressive tests, the machine arm head displacement was registered with crosshead signals (resolution: 0.1 μm). Contributions of crosshead deformation in the registered displacement were compensated with a calibration test. This calibration test involved a compressive specimen of tungsten carbide (high elastic modulus). A compressive calibration test was done for this specimen reaching a maximum load of 5 kN. The load-displacement curve obtained from this calibration test was subtracted from the subsequent compressive tests of the PVC specimens. The compressive PVC specimens had a length of 10.0 mm.

A first compressive test was done to estimate the mechanical properties of the rod bar with a controlled displacement of 0.5 mm/min. Fig. 6 shows the engineering stress vs. engineering strain curve registered after the compressive test and Table 2 includes the mechanical properties obtained from this test.

Experimental compressive creep recovery tests were performed identifying four steps:

(a) Step 1. Compressive controlled displacement at 0.5 mm/min until reach a specific load P_i.
(b) Step 2. Constant load P_i for 15 min.
(c) Step 3. Unloading controlled displacement at 0.5 mm/min until reach $P_0 = 1$ N.
(d) Step 4. Constant load P_0 for 15 min.

Table 1
Mechanical properties of the hypothetical materials.

Mat erial ID	α	τ (min)	E (MPa)	Υ	σ_y (MPa)
HM1A	0.1	1	3000	0.30	50
HM1B	0.1	5			
HM2A	0.2	1			
HM2B	0.2	5			
HM3A	0.3	1			
HM3B	0.3	5			
HM4A	0.4	1			
HM4B	0.4	5			

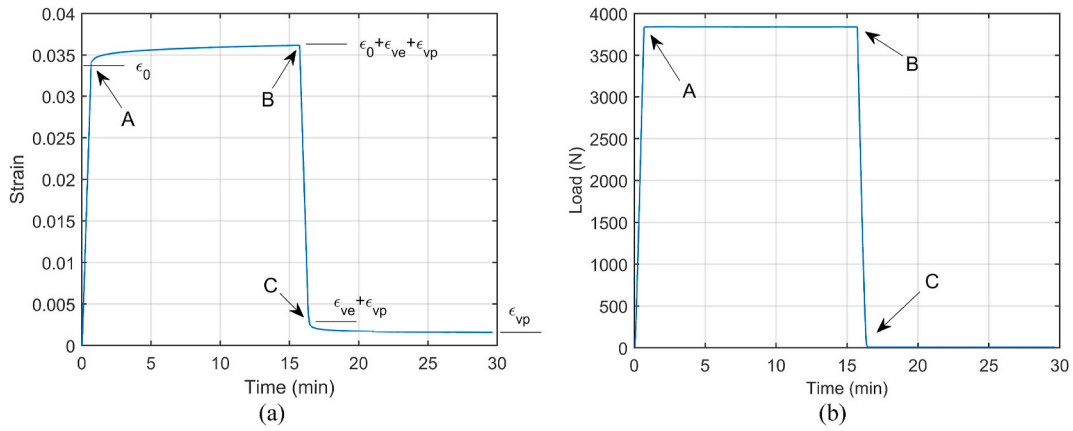

Fig. 3. (a) Strain vs. time curve and (b) load vs. time curve of a standard creep recovery test.

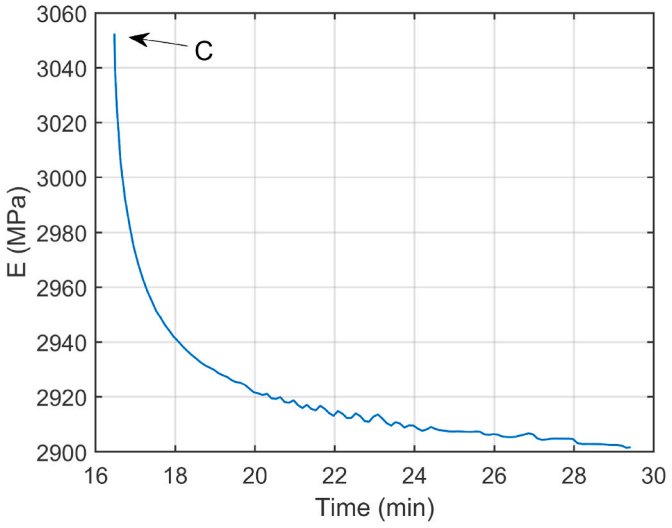

Fig. 4. Time-dependent elastic modulus vs. time curve for the recovery phase of a standard creep recovery test.

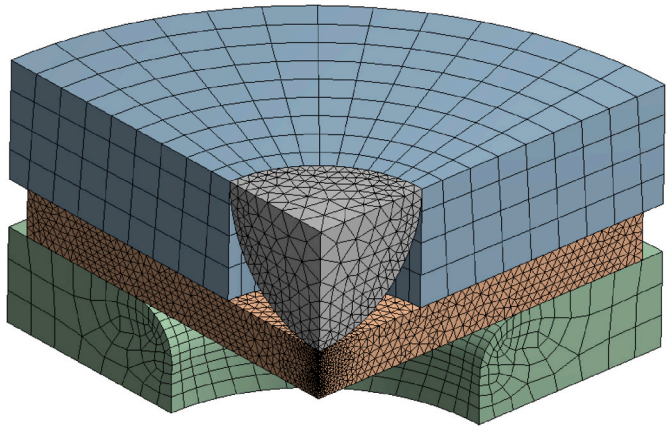

Fig. 5. Meshing for the SPT simulation.

The novel SPCRTwere performed following the next steps:

(a) Step 1. Punch displacement of 0.1 mm/min until reach a punch displacement of 0.1 mm.
(b) Step 2. Constant load P_i equal to the maximum load reached at step 1 during x minutes.

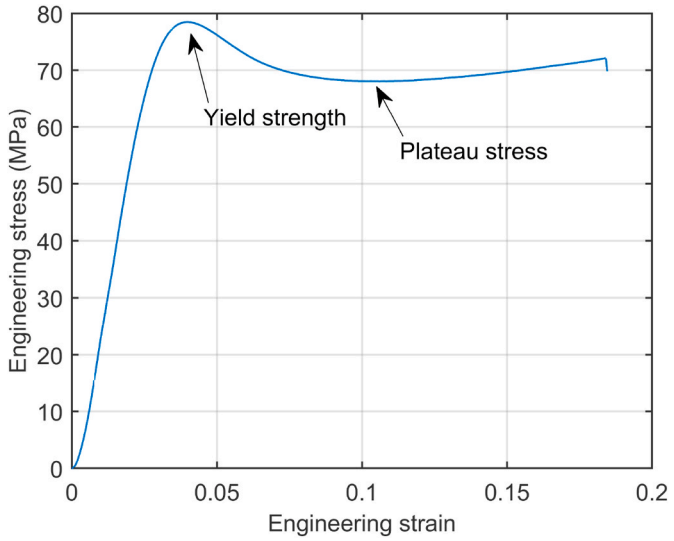

Fig. 6. Engineering stress vs. engineering strain of the compressive test for PVC rod bar.

Table 2
Mechanical properties of the PVC rod bar.

Young's modulus (MPa)	Yield strength (MPa)	Plateau stress (MPa)
3080	78.5	68.0

(c) Step 3. Unloading controlled punch displacement of 0.1 mm/min until reach $P_0 = 0.2$ N.
(d) Step 4. Constant load P_0 for x minutes.

In SPCRTs different x values were analyzed: 15, 30, and 60 min.

3. Results and discussion

3.1. Numerical FEM analysis

Fig. 7(a) shows the punch load-displacement curve of step 1, defined in the previous section, where the puncher is displaced 0.10 mm in 0.1 s. The simulation provided a maximum load of 14.8 N, which was fixed during step 2. Fig. 6(b) shows the punch displacement vs. time curves for the hypothetical material HM1A and different recovery times (60, 90, 120, 240, and 600 s). In any creep recovery test, it is necessary to establish enough creep and recovery times to saturate the viscoelastic

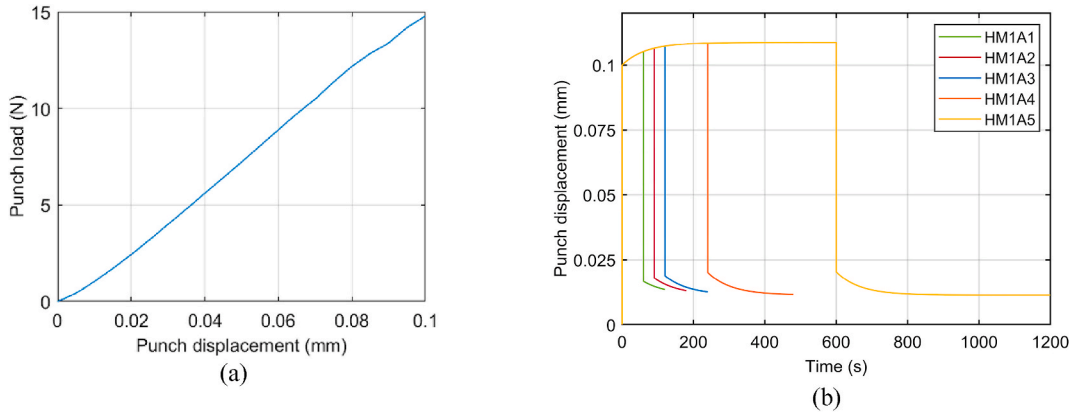

Fig. 7. (a) Loading step of the SPCRT for the hypothetical materials; (b) Punch displacement vs. time curves of the SPCRTs for the hypothetical material HM1A and different recovery times.

capability of the material. This limit is reached in the simulation when an asymptotic value is obtained during the creep step of the creep recovery test.

The time-dependent stiffness k of the recovery phase is calculated based on equation (9) and adapted to the SPCRT (see equation (11)). Fig. 8 shows the time-dependent stiffness obtained from the SPCRTs of Fig. 7(b) and equation (11).

$$k(t) = \frac{P_B}{\delta_B - \delta(t)} \quad t \geq t_C \tag{11}$$

where.

$k(t)$ is the time-dependent stiffness of the recovery phase.

P_B is the maximum load reached in the creep phase,

δ_B is the punch displacement at the end of the creep phase,

$\delta(t)$ is the punch displacement during the recovery phase ($t \geq t_C$),

t_C is the test time when the recovery phase is initiated.

Equation (10) for the time-dependent elastic modulus of the recovery phase in standard creep recovery tests, was adapted to its use for the simulation of the SPCRT (see equation (12); a single Prony component was used ($M = N = 1$) because the hypothetical materials were designed with a single Prony component). α and τ components were estimated with a non-linear-least square regression using the equation (12) and data from Fig. 7.

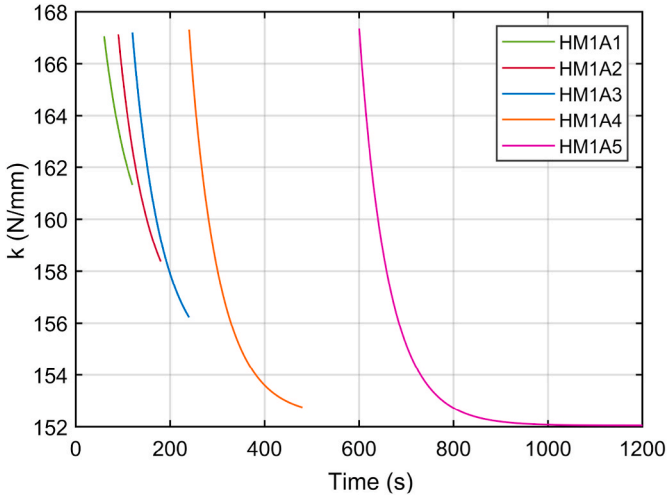

Fig. 8. Time-dependent stiffness vs. time curve for the recovery phase of SPCRTs for the hypothetical material HM1A.

$$k(t) = \frac{P_B}{\delta_B - \delta_C}\left[1 - \alpha\left(1 - e^{-\frac{t-t_C}{\tau}}\right)\right] \tag{12}$$

where P_B, δ_B, δ_C, and t_C were obtained from SPCRT curves (Fig. 7(b)).

Table (3) shows the estimated Prony components α and τ from SPCRT simulations for the HM1A material. These results pointed out the importance of establishing enough creep and recovery times during a creep recovery test or SPCRT. Although the τ component was accurately estimated for all creep times, the α component needed the saturation of the viscoelastic capability for the applied load P_B. These simulations showed a necessary creep time of 10× the relaxing time τ to estimate a fulfilling α component.

For the remainder hypothetical materials, a creep time equal to 10× the τ component was applied. Fig. 9 shows the SPCRT curves for these simulations. Fig. 10 shows the time-dependent stiffness k calculated with the equation (11) and data from Fig. 9. Applying the equation (12), a non-linear-least squares regression was applied to estimate the Prony components for each hypothetical material (see Table 4). These results showed the applicability of the SPCRT as a miniature testing method to estimate the viscoelastic properties of polymeric materials.

3.2. Experimental tests

As mentioned in the methodology section, compressive creep recovery tests and SPCRTs were performed in a rod bar of PVC. Fig. 11 shows the strain-time curves of the compressive tests for seven applied stresses σ = (6.3, 18.3, 30.0, 45.8, 60.0, 65.9, 67.0) MPa. A creep time and recovery time equal to 15 min were established in these tests. Fig. 12 represents the time-dependent elastic moduli obtained using equation (9) and data included in Fig. 11. A non-linear-least-squares regression based on equation (10) was applied with one ($M = N = 1$) and two ($M = N = 2$) Prony components. For this polymer, the best-fitted Prony series was calculated with two Prony components (see Fig. 12). Table 5 shows the calculated Prony components for each applied stress and Fig. 13 shows the sum of the α's and each τ component versus the applied stress.

Table 3
Estimated Prony components from the SPCRT simulation.

Material ID	Estimated Prony components			Real Prony components	
	A	τ (s)	R^2	α	τ (s)
HM1A1	0.05414	59.99	1	0.1	60
HM1A2	0.06742	60.25	1		
HM1A3	0.07575	60.19	1		
HM1A4	0.0884	60.92	0.9999		
HM1A5	0.09126	61.92	0.9998		

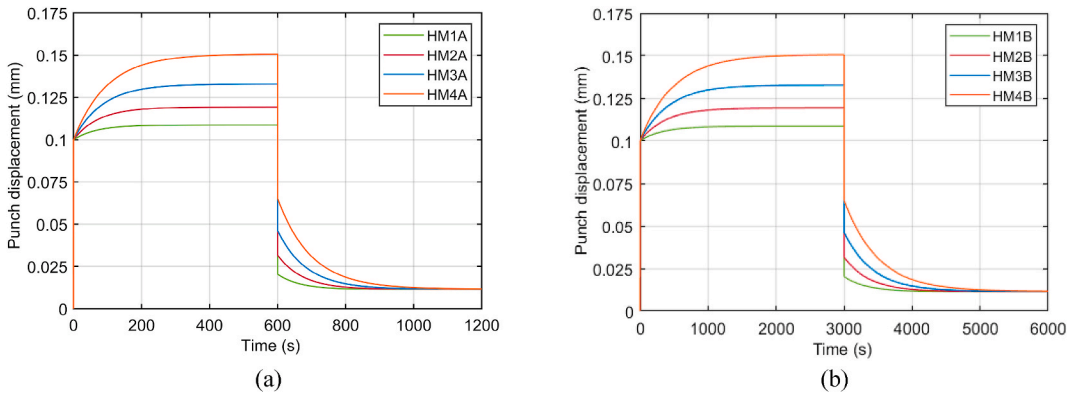

Fig. 9. Punch displacement vs. time curves of the SPCRTs for the hypothetical materials: (a) materials with relaxation times τ of 60 s; (b) materials with relaxation times τ of 300 s.

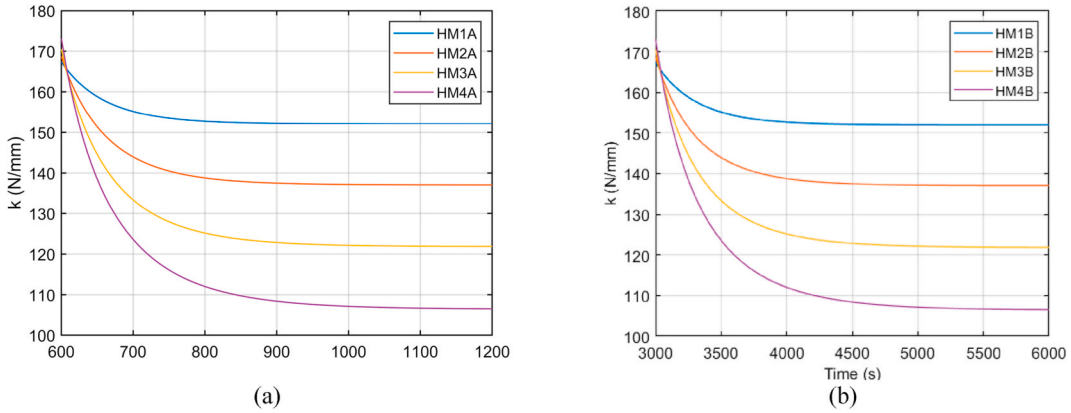

Fig. 10. Time-dependent stiffness vs. time curve for the recovery phase of SPCRTs for the hypothetical materials.

Table 4
Estimated Prony components from the SPCRT simulation.

Material ID	Estimated Prony components			Real Prony components	
	A	τ (s)	R^2	A	τ (s)
HM1A	0.0913	61.9	0.9998	0.1	60
HM1B	0.0913	309.6	0.9998	0.1	300
HM2A	0.1866	64.3	0.9994	0.2	60
HM2B	0.1867	321.7	0.9994	0.2	300
HM3A	0.2833	67.6	0.9986	0.3	60
HM3B	0.2834	338.1	0.9987	0.3	300
HM4A	0.3723	74.7	0.9985	0.4	60
HM4B	0.3810	355.4	0.9975	0.4	300

It would point out that τ components did not show significant changes with changes in the applied stress, but α components showed a stable behavior with applied stress up to the plateau stress (68.0 MPa; see Fig. 6). Thus, the viscoelastic behavior of PVC is stable for the elastic region of the material, but just when the plateau stress is reached a significant change in the viscoelastic properties is shown. PVC showed an increment in its viscoelasticity when a previous creep phase is established with applied stress near the elastic-plastic transition. In conclusion, both viscoplastic and viscoelastic properties showed a significant increment near this elastic-plastic transition. It seems to be two shelves: a lower shelf with low viscoelastic properties for elastic creep phases in creep recovery tests, and an upper shelf with high viscoelastic properties for plastic creep phases.

Fig. 14 shows the SPCRTs curves (punch displacement versus time) for the PVC for three creep and recovery times (15, 30, and 60 min). The time-dependent stiffness of the recovery phase was obtained from the

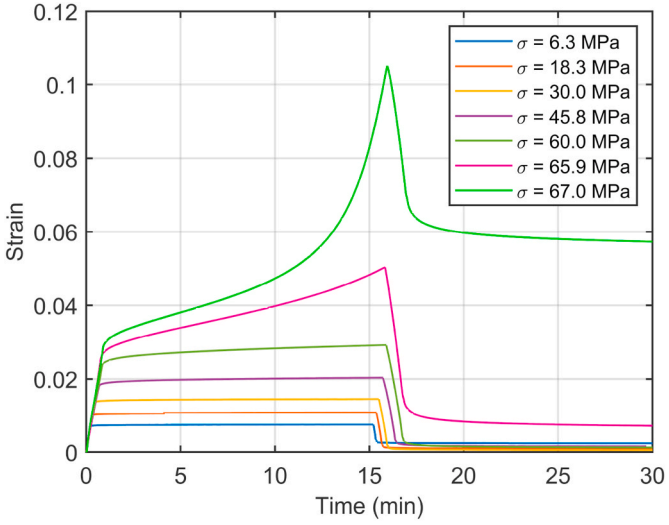

Fig. 11. Strain vs. time curves of the compressive creep recovery tests for PVC.

recovery phase of these SPCRTs and using the equation (11) (see Fig. 15). Applying the equation (12), a non-linear-least squares regression was applied to estimate the Prony components for the PVC and each recovery phase (see Table 6).

Fig. 16 represents the Prony series with the equation (10), using an elastic modulus E_C equal to the elastic modulus obtained from the compressive test (E = 3080 MPa; Table 2) and (α_i, τ_i) equal to the

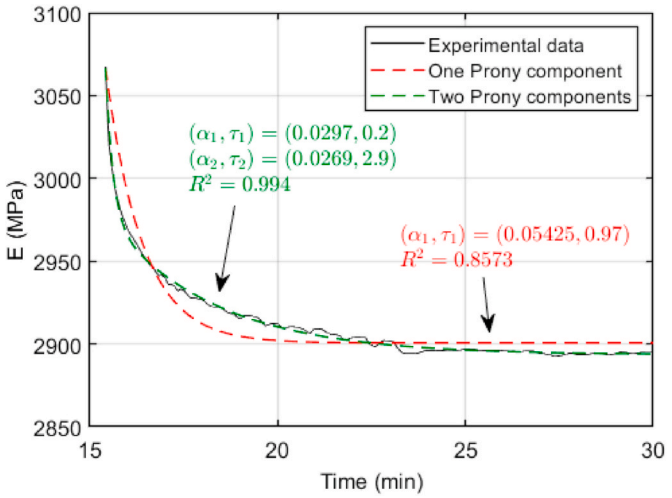

Fig. 12. Time-dependent elastic modulus vs. time curve for the recovery phase of the $\sigma = 6.3$ MPa creep recovery test.

Table 5
Estimated Prony components for each applied stress in PVC.

Stress (MPa)	α_1	α_2	τ_1 (min)	τ_2 (min)	R^2
6.3	0.02969	0.02692	0.20020	2.899	0.994
18.3	0.03413	0.02553	0.05772	2.637	0.986
30.0	0.02818	0.01900	0.22180	3.744	0.994
45.8	0.02725	0.02159	0.25860	2.897	0.996
60.0	0.03720	0.02460	0.25990	3.508	0.997
65.9	0.06790	0.05755	0.38440	4.215	0.999
67.0	0.11020	0.10340	0.31850	3.822	0.999

estimated values from the SPCRTs (Table 6). The Prony series estimated from compressive creep recovery tests for applied stresses of 6.3 MPa (viscoelastic lower shelf) and 67.0 MPa (apparent viscoelastic upper shelf) have also been included as dashed lines. SPCRTs performed for three different creep times gave similar Prony series, and these curves were contained between both estimated Prony series from the compressive creep recovery tests. This behavior is consistent, because the stress field contained in the SPCRT specimen is a combination of low stresses at outer diameters (Prony series similar to the compressive creep recovery tests performed at low stresses), and high stresses at inner diameter (Prony series over the elastic-plastic transition observed in Fig. 13). Thus, the Prony series estimated with the SPCRT should be contained between the set of Prony series estimated with the compressive creep recovery tests.

As mentioned in the experimental compressive creep recovery tests, PVC seemed to show two shelves in its viscoelastic properties: a lower shelf, clearly defined with Prony series of low and constant α's; and an upper shelf, where it is not clear what is the upper limit of the relative moduli α's for the viscoelastic Prony series. To quantify this upper viscoelastic shelf, a FEM simulation of the SPCRT for the specific experimental case of the evaluated PVC was performed considering the next assumptions:

(a) There are two viscoelastic behaviors: a lower shelf, defined by the Prony series of the compressive creep recovery test for applied stress up to 60–68 MPa; and an upper shelf, defined by a Prony series with very high and unknown α's. τ values were considered equal to the coefficients estimated in the compressive creep recovery test for applied stress of $\sigma = 6.3$ MPa because Table 5 shows no dependency between τ values and applied stress.
(b) It is assumed that the volume of the SPCRT specimen with stresses up to the plateau stress (68 MPa) is ruled by the lower shelf Prony series, and specimen volume with stresses higher than the plateau stress is ruled by the upper shelf.
(c) A FEM simulation of an SPT with the elastic-plastic properties of PVC estimated in Table 2 was launched up to a punch displacement of 0.1 mm, to obtain the load $P_{0.1}$ reached at this displacement and the yielded volume in the SPT specimen (see Fig. 17(a), where red color represents the yielded volume and blue color identifies the remainder elastic zone).
(d) The geometry of the SPCRT specimen for the viscoelastic simulation was divided into two zones (see Fig. 17(b)) like the red-

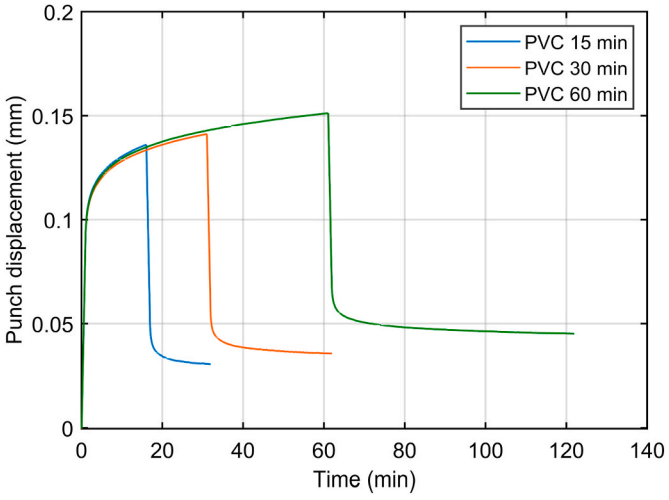

Fig. 14. Punch displacement vs. time curves of the SPCRTs for PVC.

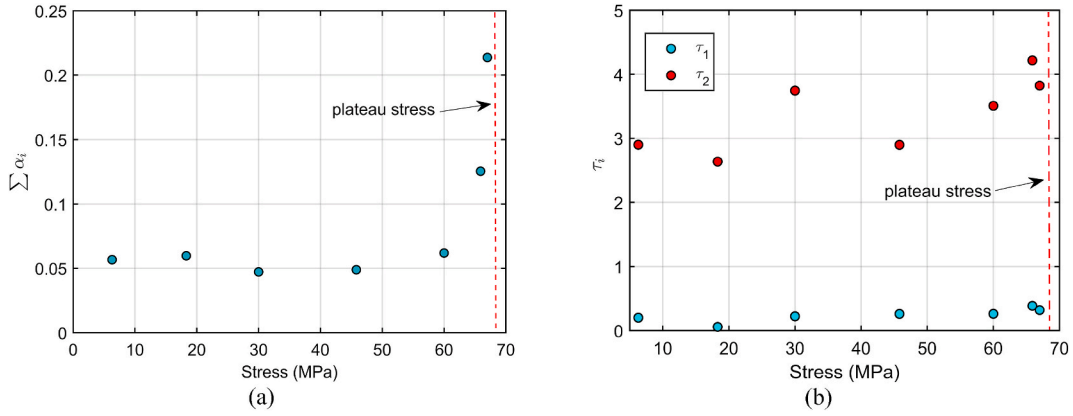

Fig. 13. (a) Sum of relative moduli, and (b) relaxation times, for each estimated Prony series in PVC.

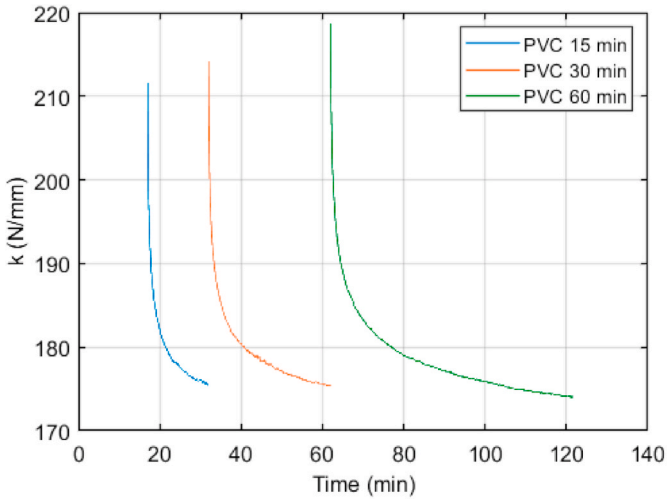

Fig. 15. Time-dependent stiffness vs. time curve for the recovery phase of SPCRT for PVC.

Table 6
Estimated Prony components for each relaxation phase in PVC.

Relaxation phase time (min)	α_1	α_2	τ_1 (min)	τ_2 (min)	R^2
15	0.0957	0.0740	0.298	3.597	0.998
30	0.1089	0.0709	0.391	7.163	0.994
60	0.1274	0.0757	0.691	14.780	0.992

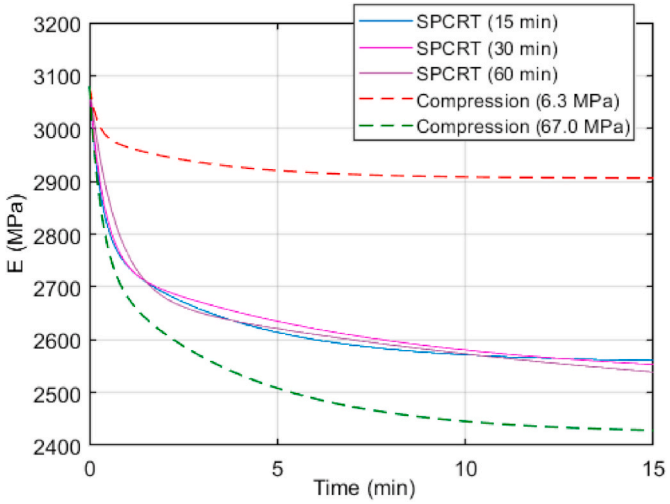

Fig. 16. Time-dependent elastic modulus vs. time curve for the estimated Prony series with experimental SPCRTs and compressive creep recovery tests.

blue zones estimated in the FEM simulation performed on (c). Lower shelf viscoelastic Prony series was established for the elastic zone, and the specimen volume just under the puncher was simulated iteratively with different values for α_1 and α_2 until emulating the experimental results included in Fig. 16 for the SPCRTs.

After the iterative set of FEM simulations detailed on (d), Fig. 18(a) represents the time-dependent elastic modulus vs. time curves for the SPCRT simulation of PVC (defined with two viscoelastic behaviors: upper and lower shelves; green curve), and compared with the experimental SPCRTs of PVC (grey curves, shown previously in Fig. 16). This figure also includes the lower shelf of Prony series (defined by estimated Prony components in the compressive creep recovery test at $\sigma = 6.3$ MPa and used in the SPCRT simulation of PVC; red dashed curve), and for the upper shelf of Prony series (defined by the iterative set of FEM simulations detailed on (d) for the SPCRT simulation of PVC; blue dashed curve). The combination of both upper and lower shelves of the Prony series on SPCRT simulation of PVC accurately simulated the experimental SPCRT curves (see green and grey curves of Fig. 18(a)). The upper shelf of Prony series (blue curve), in order to reach this approximation, was equal to $(\alpha_1,\alpha_2) = (0.25, 0.17)$ and $(\tau_1,\tau_2) = (0.2, 2.8)$. The sum of the α_i Prony components of the upper shelf, $0.25 + 0.17 = 0.42$, shows that the viscoelastic properties of PVC changes abruptly when a previous creep phase with stresses near or greater than the plateau stress (68 MPa) is established. Fig. 18(b) shows the punch displacement vs. time of the simulated SPCRT for PVC (blue curve) and the recovery phase of the experimental SPCRT for PVC with a creep time of 15 min (red dashed curve; the whole curve is shown in Fig. 14). Both recovery curves followed a similar shape. Thus, the SPCRT simulation accurately followed the experimental ones.

4. Conclusions

This paper approached the characterization of viscoelastic properties with the Small Punch Test. FEM simulations of hypothetical materials were used to understand relationships between the registered data during an SPT (punch load and punch displacement) and the viscoelastic properties of materials, and a novel Small Punch Creep Recovery Test (SPCRT) was designed to estimate an equivalent Prony series that followed or predicted the viscoelastic behavior of polymeric materials. Experimental tests (compressive creep recovery tests and SPCRTs) were performed in a rod bar of PVC to verify the findings reached in the FEM simulations. The most important conclusions derived from this investigation were:

(a) Numerically, the SPT and its adapted test named as Small Punch Creep Recovery Test (SPCRT) showed outstanding capabilities for estimating viscoelastic properties of polymeric materials.
(b) For its implementation, the most important stamping block was the heterogeneous stress field that supports the SPT specimen along with the test. Materials that show high-dependent viscoelasticity with the applied stress during the creep phase will show a mean or intermediate value of these changing viscoelastic properties when it is tested with the SPCRT. It does not mean a non-applicability of the SPCRT for these materials, but it is important to clarify that the estimated viscoelastic properties would be equivalent to an intermediate value of this stress-dependent viscoelasticity.
(c) PVC polymer showed stress-independent viscoelasticity up to the plateau stress. This stability showed an abrupt change in the proximity to this specific stress, with a notorious increment in the viscoelastic properties. This is equivalent to the influence of glass transition temperature T_g in the viscoelasticity of amorphous polymers. Assuming that applied elastic stress implies internal elastic energy provided to the material, it could be possible to reach a stress limit (the plateau stress) equivalent to an elastic energy limit that was enough to initiate a broking-reforming of the secondary molecular bonds during the creep phase. Molecules slide past each other with relative ease and viscoelastic behavior could be facilitated and accumulated during this creep phase. During the recovery phase, this extra viscoelasticity would be recovered, showing the differential viscoelastic properties up to and over the plateau stress. Due to the inherent instability of the compressive creep recovery tests at these stress levels, it is almost impracticable to perform long creep phases with this testing method. But the SPT and the SPCRT show implicit stability for these stress levels. Through iterative FEM simulations and experimental SPCRTs, the viscoelastic properties of PVC at high-

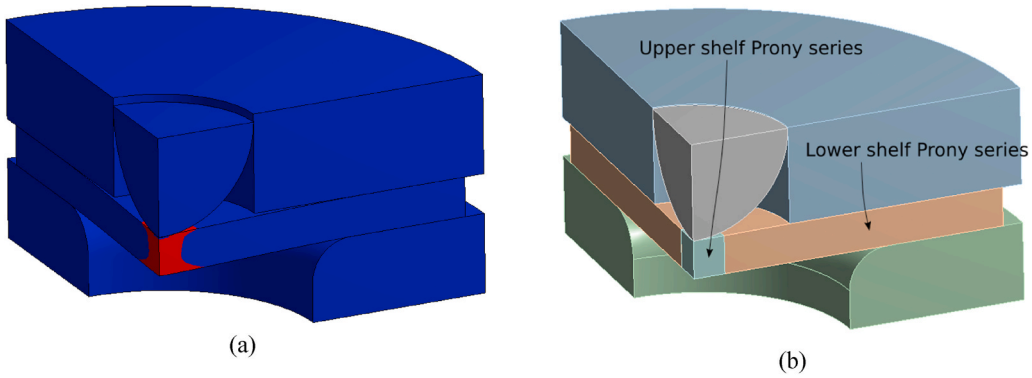

Fig. 17. FEM simulations for PVC: (a) SPT with a punch displacement of 0.1 mm and elastic-plastic material properties (red region: yielded zone; blue region: elastic zone); (b) geometry of the SPCRT with two volumes in the SPT specimen. (For interpretation of the references to color in this figure legend, the reader is referred to the Web version of this article.)

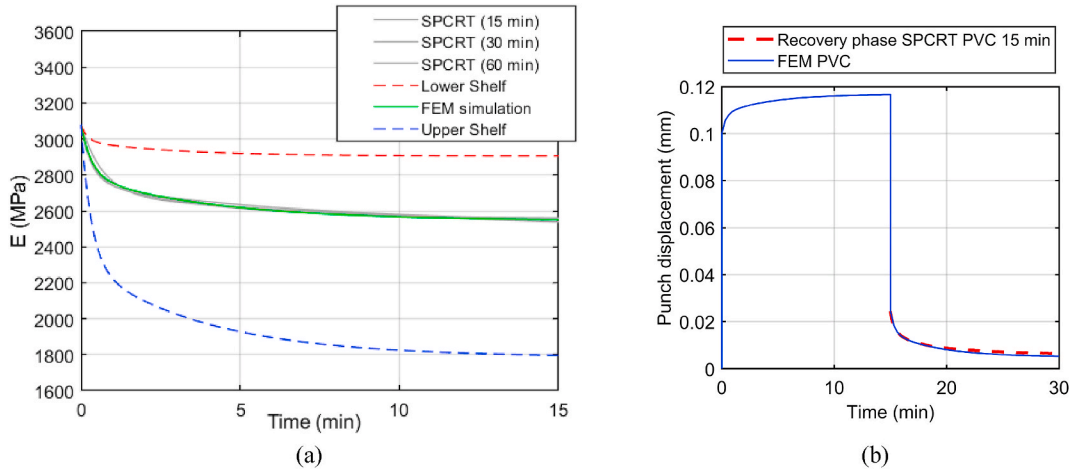

Fig. 18. (a) Time-dependent elastic modulus vs. time curve for the estimated Prony series with experimental SPCRTs, simulated SPCRT and estimated upper and lower shelves of the Prony series for PVC; (b) Punch displacement vs. time curve of the simulated SPCRT for PVC (blue curve) and the recovery phase of the experimental SPCRTs for PVC with a creep time of 15 min (red dashed curve). (For interpretation of the references to color in this figure legend, the reader is referred to the Web version of this article.)

stress fields were estimated. The estimated Prony components for the viscoelasticity of PVC were:

a. Lower shelf of Prony series: $(\alpha_1,\alpha_2) = (0.0297, 0.0269)$ and $(\tau_1,\tau_2) = (0.2, 2.8)$ for stresses up to 68 MPa.
b. Upper shelf of Prony series: $(\alpha_1,\alpha_2) = (0.25, 0.17)$ and $(\tau_1,\tau_2) = (0.2, 2.8)$ for stresses over 68 MPa.

Data availability

The raw/processed data required to reproduce these findings cannot be shared at this time as the data also forms part of an ongoing study.

Author statement

Jose Calaf-Chica: Conceptualization, Methodology, Software, Writing- Original draft, Investigation, Formal analysis; P.M. Bravo Díez: Validation, Resources, Writing - Review & Editing, Supervision, Project administration; M. Preciado Calzada: Data Curation, Investigation, Writing - Review & Editing.

Declaration of competing interest

The authors declare that they have no known competing financial interests or personal relationships that could have appeared to influence the work reported in this paper.

References

ASTM, 2008. F2183 - 02: Standard Test Method for Small Punch Testing of Ultra-High Molecular Weight Polyethylene Used in Surgical Implants 1. ASTM Book of Standards, pp. 1–5, 13.01(Reapproved 2008.

ASTM, 2013a. F2977-13: Standard Test Method for Small Punch Testing of Polymeric Biomaterials Used in. ASTM Book of Standards, pp. 14–18. https://doi.org/10.1520/E3205-20, 13.02.

ASTM, 2013b. F2977-13: Standard Test Method for Small Punch Testing of Polymeric Biomaterials Used in. ASTM Book of Standards, pp. 14–18, 13.02.

Altstadt, E., Houska, M., Simonovski, I., Bruchhausen, M., Holmström, S., Lacalle, R., 2018. On the estimation of ultimate tensile stress from small punch testing. Int. J. Mech. Sci. 136, 85–93. https://doi.org/10.1016/j.ijmecsci.2017.12.016.

Altstadt, E., Bergner, F., Houska, M., 2021. Use of the small punch test for the estimation of ductile-to-brittle transition temperature shift of irradiated steels. Nuclear Mater. Energy 26, 100918. https://doi.org/10.1016/j.nme.2021.100918.

Bruchhausen, M., Holmström, S., Simonovski, I., Austin, T., Lapetite, J.M., Ripplinger, S., de Haan, F., 2016. Recent developments in small punch testing: tensile properties and DBTT. Theor. Appl. Fract. Mech. 86, 2–10. https://doi.org/10.1016/j.tafmec.2016.09.012.

Calaf-Chica, J., Bravo Díez, P.M., Preciado Calzada, M., Garcia-Tarrago, M.J., 2020. Optimization of the t/10 offset correlation method to obtain the yield strength with the Small Punch Test. J. Nucl. Mater. 534, 152177. https://doi.org/10.1016/j.jnucmat.2020.152177.

Calaf Chica, J., Bravo Diez, P.M., Preciado Calzada, M., Garcia Tarrago, M.J., 2021. Implementation of the small punch test for the mechanical properties estimation of aluminum alloys. Dyna 96 (1), 79–84. https://doi.org/10.6036/9747.

Cao, Y., Mohamed, A.M., Moshtaghi, S., Taheri, M., Torkamany, M.J., 2021. Investigation of creep behavior of Ni3Al-base superalloy by small punch creep. Vacuum 187, 110101. https://doi.org/10.1016/j.vacuum.2021.110101.

Chen, H., Yang, R., Al-Abedy, H.K., Li, H., Sun, W., Jones, I.A., 2020. Characterisation of deformation process and fracture mechanisms of P91 steel at 600 °C in small punch tensile testing. Mater. Char. 168, 110514. https://doi.org/10.1016/j.matchar.2020.110514.

Chica, J.C., Bravo Díez, P.M., Preciado Calzada, M., 2017. Improved correlation for elastic modulus prediction of metallic materials in the Small Punch Test. Int. J. Mech. Sci. 134, 112–122. https://doi.org/10.1016/j.ijmecsci.2017.10.006.

Edidin, A.A., Kurtz, S.M., 2001. Development and validation of the small punch test for UHMWPE used in total joint replacements. Key Eng. Mater. 198–199, 1–40. https://doi.org/10.4028/www.scientific.net/kem.198-199.1.

Gao, T., Ying, L., Hu, P., Han, X., Rong, H., Wu, Y., Sun, J., 2020. Investigation on mechanical behavior and plastic damage of AA7075 aluminum alloy by thermal small punch test: experimental trials, numerical analysis. J. Manuf. Process. 50, 1–16. https://doi.org/10.1016/j.jmapro.2019.12.012.

Ghodke, S.R., Dutta, B.K., Durgaprasad, P.V., 2020. Analytical development and experimental verification of empirical correlations to determine mechanical properties of copper alloys using small punch test data. Fusion Eng. Des. 159, 111786. https://doi.org/10.1016/j.fusengdes.2020.111786.

Giddings, V.L., Kurtz, S.M., Jewett, C.W., Foulds, J.R., Edidin, A.A., 2001. A small punch test technique for characterizing the elastic modulus and fracture behavior of PMMA bone cement used in total joint replacement. Biomaterials 22 (13), 1875–1881. https://doi.org/10.1016/S0142-9612(00)00372-0.

Hurst, R., Li, Y., Turba, K., 2019. Determination of fracture toughness from the small punch test using circular notched specimens. Theor. Appl. Fract. Mech. 103, 102238. https://doi.org/10.1016/j.tafmec.2019.102238.

Jaekel, D.J., MacDonald, D.W., Kurtz, S.M., 2011. Characterization of PEEK biomaterials using the small punch test. J. Mech. Behav. Biomed. Mater. 4 (7), 1275–1282. https://doi.org/10.1016/j.jmbbm.2011.04.014.

Karthik, V., Kasiviswanathan, K.V., Raj, B., 2016. Miniaturized testing of engineering materials. In: Miniaturized Testing of Engineering Materials. https://doi.org/10.1201/9781315372051.

Koga, Y., Arao, Y., Kubouchi, M., 2020. Application of small punch test to lifetime prediction of plasticized polyvinyl chloride wire. Polym. Degrad. Stabil. 171, 109013. https://doi.org/10.1016/j.polymdegradstab.2019.109013.

Kurtz, Steven M., Foulds, J.R., Jewett, C.W., Srivastav, S., Edidin, A.A., 1997. Validation of a small punch testing technique to characterize the mechanical behaviour of ultra-high-molecular-weight polyethylene. Biomaterials 18 (24), 1659–1663. https://doi.org/10.1016/S0142-9612(97)00124-5.

Kurtz, S.M., Siskey, R., Reitman, M., 2010. Accelerated aging, natural aging, and small punch testing of gamma-air sterilized polycarbonate urethane acetabular components. J. Biomed. Mater. Res. B Appl. Biomater. 93 (2), 442–447. https://doi.org/10.1002/jbm.b.31601.

Lancaster, R.J., Harrison, W.J., Norton, G., 2015. An analysis of small punch creep behaviour in the γ titanium aluminide Ti-45Al-2Mn-2Nb. Mater. Sci. Eng. 626, 263–274. https://doi.org/10.1016/j.msea.2014.12.045.

Lancaster, R.J., Jeffs, S.P., Illsley, H.W., Argyrakis, C., Hurst, R.C., Baxter, G.J., 2019. Development of a novel methodology to study fatigue properties using the small punch test. Mater. Sci. Eng. 748, 21–29. https://doi.org/10.1016/j.msea.2019.01.074.

Lewis, D.T.S., Lancaster, R.J., Jeffs, S.P., Illsley, H.W., Davies, S.J., Baxter, G.J., 2019. Characterising the fatigue performance of additive materials using the small punch test. Mater. Sci. Eng. 754, 719–727. https://doi.org/10.1016/j.msea.2019.03.115.

Li, Y., Matocha, K., Hurst, R., Čižek, P., Turba, K., Stevens, P., 2019. Experimental verification to determine fracture toughness from the small punch test using "Local approach. Theor. Appl. Fract. Mech. 102, 16–29. https://doi.org/10.1016/j.tafmec.2019.03.015.

Manahan, M.P., Argon, A.S., Harling, O.K., 1981. The development of a miniaturized disk bend test for the determination of postirradiation mechanical properties. J. Nucl. Mater. 104 (C), 1545–1550. https://doi.org/10.1016/0022-3115(82)90820-0.

Maspoch, M.L., Santana, O.O., Cailloux, J., Franco-Urquiza, E., Rodriguez, C., Belzunce, J., Martínez, A.B., 2015. Ductile-brittle transition behaviour of PLA/o-MMT films during the physical aging process. Express Polym. Lett. 9 (3), 185–195. https://doi.org/10.3144/expresspolymlett.2015.20.

Rasche, S., Strobl, S., Kuna, M., Bermejo, R., Lube, T., 2014. Determination of strength and fracture toughness of small ceramic discs using the small punch test and the ball-on-three-balls test. Procedia Mater. Sci. 3, 961–966. https://doi.org/10.1016/j.mspro.2014.06.156.

Rodríguez, C., Arencón, D., Belzunce, J., Maspoch, M.L., 2014. Small punch test on the analysis of fracture behaviour of PLA-nanocomposite films. Polym. Test. 33, 21–29. https://doi.org/10.1016/j.polymertesting.2013.10.013.

Rodríguez, C., Cuesta, I.I., Maspoch, M.L.L., Belzunce, F.J., 2016. Application of the miniature small punch test for the mechanical characterization of polymer materials. Theor. Appl. Fract. Mech. 86, 78–83. https://doi.org/10.1016/j.tafmec.2016.10.001.

Shindo, Y., Narita, F., Horiguchi, K., Magara, Y., Yoshida, M., 2003. Electric fracture and polarization switching properties of piezoelectric ceramic PZT studied by the modified small punch test. Acta Mater. 51 (16), 4773–4782. https://doi.org/10.1016/S1359-6454(03)00303-3.

Simonovski, I., Baraldi, D., Holmström, S., Altstadt, E., Delville, R., Bruchhausen, M., 2018. Determining the ultimate tensile strength of fuel cladding tubes by small punch testing. J. Nucl. Mater. 509, 620–630. https://doi.org/10.1016/j.jnucmat.2018.07.041.

Taheri, M., Halvaee, A., Kashani Bozorg, S.F., Golezani, A.S., Liavoli, R.P., Kashi, A.A., 2021. The effect of heat treatment on creep behavior of GTD-111 superalloy welded by pulsed Nd:YAG laser using small punch test. Eng. Fail. Anal. 122, 105255. https://doi.org/10.1016/j.engfailanal.2021.105255.

Wang, L.Y., Wang, Y.C., Zhou, Z.J., Wan, H.Y., Li, C.P., Chen, G.F., Zhang, G.P., 2020a. Small punch creep performance of heterogeneous microstructure dominated Inconel 718 fabricated by selective laser melting. Mater. Des. 195, 109042. https://doi.org/10.1016/j.matdes.2020.109042.

Wang, W., Zhong, J., Zhang, X., Jiang, T., Guan, K., 2020b. Study of estimation of ductile-brittle transition temperature using U-notched small punch test specimens. Theor. Appl. Fract. Mech. 108, 102627. https://doi.org/10.1016/j.tafmec.2020.102627.

Xue, L., Ling, X., Yang, S., 2019. Mechanical behaviour and strain rate sensitivity analysis of TA2 by the small punch test. Theor. Appl. Fract. Mech. 99, 9–17. https://doi.org/10.1016/j.tafmec.2018.11.002.

Yang, S.S., Ling, X., Qian, Y., Ma, R.B., 2015. Yield strength analysis by small punch test using inverse finite element method. Procedia Eng. 130, 1039–1045. https://doi.org/10.1016/j.proeng.2015.12.259.

Yao, C.F., Dai, Y., 2021. DBTT shift of Optifer-IX, Eurofer 97 and MA956 steels after irradiation evaluated with small punch tests. J. Nucl. Mater. 544, 152725. https://doi.org/10.1016/j.jnucmat.2020.152725.